

RESEARCH ARTICLE

Luminescence study of LiMgBO₃:Dy for γ -ray and carbon ion beam exposure

Mangesh M. Yerpude¹ | Vibha Chopra²  | N.S. Dhoble³ | R.M. Kadam⁴ |
Aleksander R. Krupski⁵ | S.J. Dhoble¹ 

¹Department of Physics, R.T.M. Nagpur University, Nagpur 440033, India

²P.G. Department of Physics and Electronics, DAV College, Amritsar 143001, Punjab, India

³Department of Chemistry, Sevalal Mahila Mahavidyalaya, Nagpur 440009, India

⁴Radiochemistry Division, Bhabha Atomic Research Centre, Trombay, India

⁵Faculty of Science, SEES, University of Portsmouth, Portsmouth PO1 3QL, UK

Correspondence

Vibha Chopra, P.G. Department of Physics and Electronics, DAV College, Amritsar - 143001, Punjab, India.
Email: vibhachopra04@gmail.com

Funding information

IUAC; University Grants Commission-India, Grant/Award Number: UGC-NET-JRF

Abstract

LiMgBO₃:Dy³⁺, a low Z_{eff} material was prepared using the solution combustion method and its luminescence properties were studied using X-ray diffraction (XRD), scanning electron microscopy (SEM), thermoluminescence (TL), photoluminescence (PL), Fourier transform infrared spectroscopy, and electron paramagnetic resonance (EPR) techniques. Reitveld refinement was also performed for the structural studies. The PL emission spectra for LiMgBO₃:Dy³⁺ consisted of two peaks at 478 nm due to the $^4F_{9/2} \rightarrow ^6H_{15/2}$ magnetic dipole transition and at 572 nm due to the hypersensitive $^4F_{9/2} \rightarrow ^6H_{13/2}$ electric dipole transition of Dy³⁺, respectively. A TL study was carried out for both the γ -ray-irradiated sample and the C⁵⁺ irradiated samples and was found to show high sensitivity for both. Moreover the γ -ray-irradiated LiMgBO₃:Dy³⁺ sample showed linearity in the dose range 10 Gy to 1 kGy and C⁵⁺-irradiated samples show linearity in the fluence range 2×10^{10} to 1×10^{11} ions/cm². In the present study, the initial rise method, various heating rate method, the whole glow curve method, glow curve convolution deconvolution function, and Chen's peak shape method were used to calculate kinetic parameters to understand the TL glow curve mechanism in detail. Finally, an EPR study was performed to examine the radicals responsible for the TL process.

KEYWORDS

ESR, LiMgBO₃, tissue equivalent material, trapping parameters

1 | INTRODUCTION

Boron-based materials show interesting thermoluminescence (TL) properties when exposed to ionizing radiation^[1,2]. The luminescence properties of lithium borate and magnesium borate in both microcrystalline and nanocrystalline forms have been studied previously^[1-4]. Recently, researchers who studied lithium magnesium borate phosphor found that it was useful for applications in dosimetry^[5,6].

To date, only a few studies on LiMgBO₃ have been reported^[5]. Recently, the TL properties of rare earth ion (RE = Tb, Gd, Dy, Pr, Mn, Ce, Eu)-doped lithium magnesium borate (LMB), prepared using

the solid state diffusion method, have been documented^[6]. LMB:Tb³⁺ showed the best results with a stable TL peak at 240°C. LMB:Tb³⁺ was about four times more sensitive than TLD-100. Optical properties of LMB glasses doped with Dy³⁺, Sm³⁺ ions have been studied^[7]. Photoluminescence properties of LMB:Eu and LMB:Eu,Bi have also been studied in detail^[8]. LiMgBO₃:Dy³⁺ in its polycrystalline form has been prepared using a novel solution combustion method and its TL sensitivity was found to be half compared with commercial TLD-100 and showed a high degree of fading of 30% after 20 days^[9]. Furthermore, LiMgBO₃:Dy³⁺ in its nanocrystalline form has been prepared using the combustion method and its structural and optical properties have been studied^[10].

There have been no previous reports in the published literature on the study of the luminescence properties of LMB synthesized using the solution combustion method using present precursors, and also no reports on ion beam dosimetry with the same material. Recently, in the field of cancer treatment, heavy ion radiotherapy compared with photon therapy has attracted attention^[11,12]. Heavy ions show low energy straggling and strong increase in their linear energy transfer (LET) in the affected region^[12-16]. Among the heavy ions, carbon ions are most significant due to increase in LET and the size of carbon ions is such that they cause much damage to the cancer cell, but relatively little damage to healthy cells nearby^[12]. The effective atomic number of LiMgBO_3 was calculated using the formula:

$$Z_{\text{eff}} = \sqrt[2.94]{f_1 \times (Z_1)^{2.94} + f_2 \times (Z_2)^{2.94} + f_3 \times (Z_3)^{2.94} + f_4 \times (Z_4)^{2.94}} \quad (1)$$

where.

f_n = fraction of total number of electrons associated with each element,

Z_n = atomic number of each element.

It was found that LiMgBO_3 had a low effective atomic number ($Z_{\text{eff}} \approx 8.8$) close to that of biological tissue ($Z_{\text{eff}} = 7.4$), therefore this material can be studied for its dosimetric properties. In the present study, LiMgBO_3 doped with Dy was synthesized using the solution combustion method with different starting materials than reported previously^[9]. The synthesized samples were irradiated with a γ -ray dose and their luminescence properties were studied using photoluminescence (PL) and electron paramagnetic resonance (EPR) techniques. Finally the TL characteristics of γ -ray- and C^{5+} ion beam-exposed samples were studied to find their suitability for application in radiation dosimetry.

2 | EXPERIMENTAL

2.1 | Synthesis

The solution combustion method was used to prepare Dy^{3+} activated with LiMgBO_3 . All analytical reagent (AR) grade precursors: LiNO_3 , $\text{Mg}(\text{NO}_3)_2$, H_3BO_3 , and NH_2CONH_2 were weighed in stoichiometric proportion and dissolved in double-distilled water with constant stirring. Dysprosium nitrate was added by dissolving Dy_2O_3 in dilute nitric acid at the desired concentration for doping. The prepared mixture was heated by placing on a hot plate at a constant temperature of 80°C with constant stirring. The formed gel was then transferred to a preheated muffle furnace at 500°C . An exothermic reaction took place and a white foamy powder was obtained in the crucible. The foamy powder was crushed to fine particles and was heated in a muffle furnace at 700°C for 2 h and allowed to cool slowly. Later the sample was annealed at 700°C for 1 h and quenched quickly to room temperature by putting it on a metal block. The final product obtained was studied for its different luminescence properties.

2.2 | Characterization

For characterization of the synthesized materials, X-ray diffraction (XRD), TL, PL, ESR techniques have been used. The XRD pattern was recorded using a diffractometer with $\text{Cu-K}\alpha$ radiation ($\lambda = 1.5406 \text{ \AA}$) at a 40 kV tube voltage on a Rigaku instrument with a step size of $2\theta = 0.02^\circ$. Furthermore, for SEM, a JEOL 6380 A instrument was used to study the surface morphology of the synthesized sample. Fourier transform infrared (FTIR) spectra from the prepared phosphor were recorded using a Shimadzu IR Affinity-1 spectrophotometer. PL measurements were taken using an RF-5301PC spectrofluorophotometer with a xenon lamp as the excitation source. EPR measurements were performed using a Bruker EMM-1843 spectrometer operating at an X-band frequency of 9.43 GHz. About 150 mg of $\text{LiMgBO}_3:\text{Dy}^{3+}$ sample was used to record the EPR spectra and the sample was exposed to a 1 kGy dose of γ -rays from a ^{60}Co source before EPR measurements. For the TL measurements, the synthesized samples were irradiated with γ -rays or a 75 MeV C^{5+} ion beam. γ -Ray exposure was carried out using a calibrated ^{60}Co source or C^{5+} ion beam exposure was carried out using a 16MV tandem Van de Graaff-type electrostatic accelerator (15 UD Pelletron)^[17] at

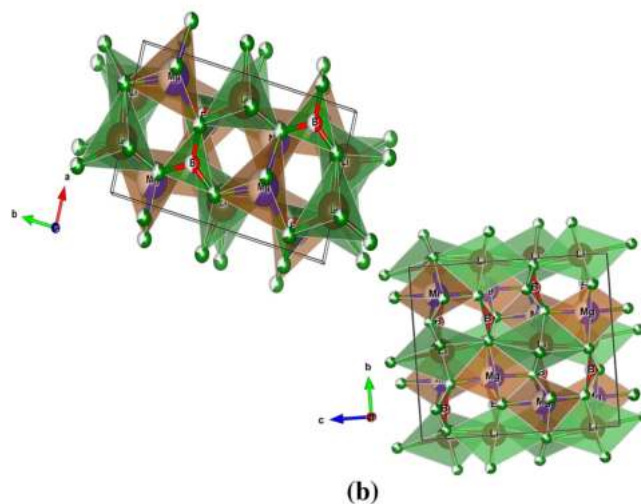
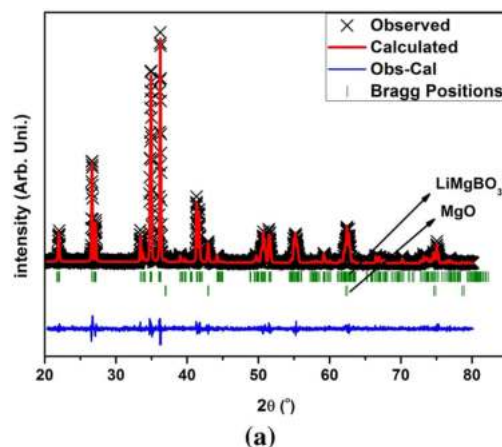


FIGURE 1 (a) Rietveld refined X-ray diffraction pattern; (b) crystal structure of monoclinic LiMgBO_3 phosphor

the Inter-University Accelerator Center (IUAC), New Delhi, India. After irradiation, TL measurements were recorded using a Nucleonix TLD reader (model: 1009I) taking 5 mg of sample every time.

3 | RESULTS AND DISCUSSION

3.1 | Structure analysis

The Rietveld refined XRD pattern of monoclinic LiMgBO_3 (97%) with a secondary cubic MgO (3%) phase is shown in Figure 1(a). The XRD pattern is consistent with the standard pattern depicting the pure monoclinic phase with space group $C2/c$ ^[10]. The diffraction peaks were indexed according to the JCPDS file (00-079-1996)^[10]. Furthermore, addition of dopant Dy^{3+} (activator) did not affect the crystal structure of the host lattice. For the determination and refinement of lattice parameters, Rietveld XRD profile fitting was performed using FULLPROF software. Initial parameters were taken from the already reported structural characterization of LiMgBO_3 ^[5]. The calculated lattice parameters were approximated to be $a = 5.168 \text{ \AA}$, $b = 8.887 \text{ \AA}$, $c = 9.916 \text{ \AA}$, $\beta = 91.20^\circ$ and $V = 455.322 \text{ \AA}^3$ ^[10]. The Rietveld refinement parameters are listed in Table 1. The crystal structure of LiMgBO_3 is shown in Figure 1(b). Norrestem *et al.* showed that the Li atom in LiMgBO_3 occupied a disordered position, allowing the lithium atom to occupy two positions around the initial average position^[5]. But, in the present study, a more ordered position for the lithium atom with bonds elongated along the c -axis was observed. The Li position has a triangular coordination using the three O atoms with very short bond distances of about 1.9 \AA , further away (about 2.7 \AA) there were two more O atoms so that a $3 + 2$ coordination in the form of an elongated trigonal bi-pyramidal coordination polyhedron was obtained. The Li and Mg atoms were five-coordinated using an oxygen atom to form a distorted trigonal bi-pyramidal coordination polyhedron.

TABLE 1 Rietveld refinement parameters for monoclinic LiMgBO_3

Empirical formula						$\text{LiMgBO}_3:\text{Dy}^{3+}$
Crystal system and space group						Monoclinic, $C2/c$ (15)
Unit cell parameters						$a = 5.168 \text{ \AA}$, $b = 8.887 \text{ \AA}$, $c = 9.916 \text{ \AA}$, $\beta = 91.22^\circ$
Volume						$V = 455.322 \text{ \AA}^3$
Calculated density						2.194 g/cm^3
Goodness of fit (χ^2)						1.41
Reliability factors						$R_p = 10.7$, $R_{wp} = 14.9$, $R_{exp} = 12.5$
Atom	x	y	z	Occupancy	B	
Li	0.1427	0.5167	0.1151	0.972	4.327	
Mg	0.1625	0.1708	0.1261	0.7635	1.571	
Dy	0.1625	0.1708	0.1261	0.0016	2.189	
B	0.1702	0.8480	0.1296	0.5941	1.443	
O ₁	0.2753	0.6939	0.1621	0.8515	2.134	
O ₂	0.3095	0.9553	0.1294	0.8565	2.382	
O ₃	0.4056	0.3299	0.0857	0.8677	2.725	

LiO_5 polyhedrons were interconnected by two oxygen atoms forming layers parallel to the c - a plane distributed along the b -axis. The MgO_5 polyhedrons shared two oxygen atoms with other MgO_5 polyhedrons forming diagonal layers. These LiO_5 and MgO_5 layers were linked together by edge and shared into zig-zag rows extending in the diagonal c - a direction. The Li and B ions linked these rows together into a three-dimensional network.

Figure 2 shows the SEM photographs from the $\text{LiMgBO}_3:\text{Dy}^{3+}$ phosphor and clearly indicated agglomeration with rod shapes distributed widely. The morphology of the powder was observed to be polycrystalline, made of microcrystalline particles. Voids and pores seen in the SEM images were due to the production of combusting gases during the sol-gel combustion process^[9].

3.2 | Fourier transform (FTIR) analysis

FTIR spectra of the synthesized phosphor $\text{LiMgBO}_3:\text{Dy}^{3+}$ prepared using the solution chemical route are displayed in Figure 3. The spectra were recorded for the mid-infrared region 400 cm^{-1} to 4000 cm^{-1} using transmittance mode. Bands at 1458 cm^{-1} and 1287 cm^{-1} corresponded to asymmetric stretching relaxations of the B-O bond in the trigonal BO_3 unit^[9]. The band at 1182 cm^{-1} showed the symmetrical stretching vibrations of a B-O bond. Bands at 1025 cm^{-1} and 836 cm^{-1} showed the bending vibrations of borate segments^[18]. Furthermore, borate deformation and plane bending of the boron-oxygen triangles were expressed by bands at 704 and 676 cm^{-1} . Finally, bands at wavelengths less than 450 cm^{-1} were attributed to lattice vibrations.

3.3 | Photoluminescence (PL)

Photoluminescence spectra were studied to confirm the state of the dopant in the host lattice. The excitation and emission spectra of

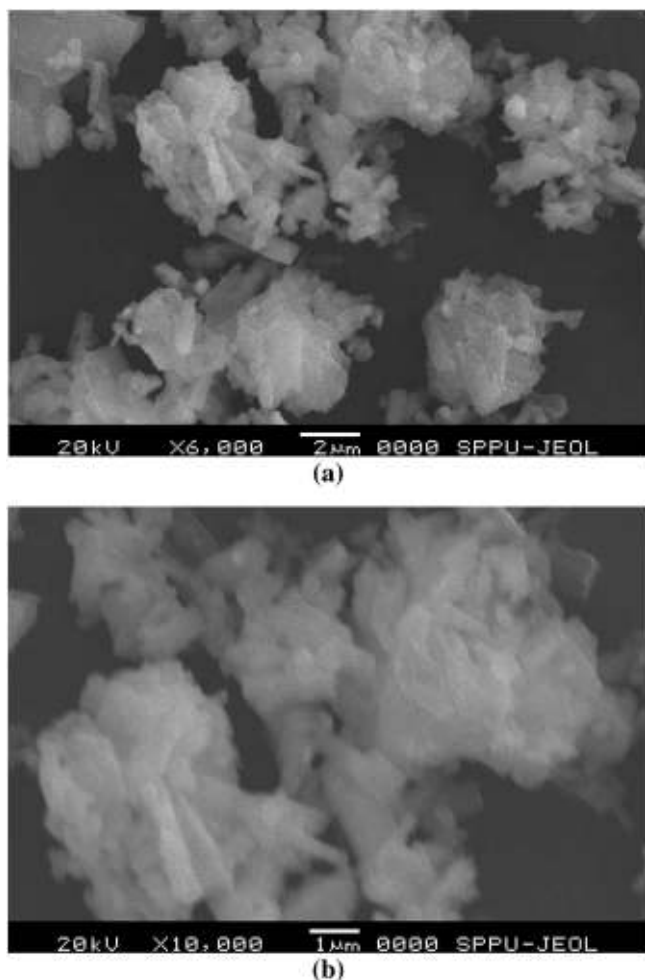


FIGURE 2 (a, b) Scanning electron microscopy micrographs of the $\text{LiMgBO}_3:\text{Dy}^{3+}$ phosphor

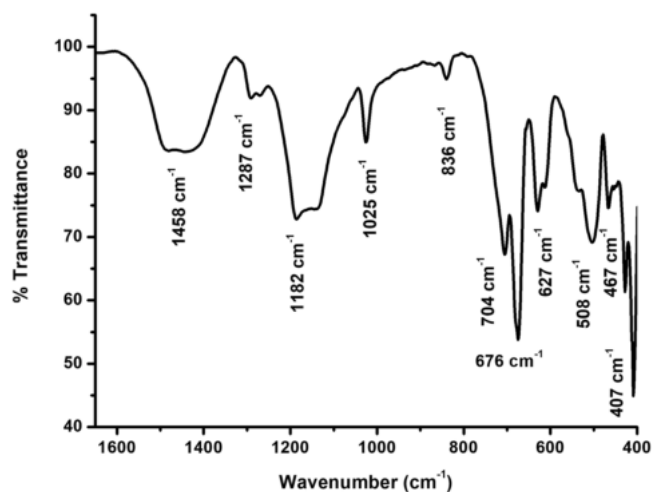


FIGURE 3 Fourier transform infrared spectrum of the synthesized $\text{LiMgBO}_3:\text{Dy}^{3+}$ phosphor

synthesized $\text{LiMgBO}_3:\text{Dy}^{3+}$ are shown in Figure 4(a) and Figure 4(b), respectively. Peaks at 323, 349, 365, 388 and 427 nm were observed in the excitation spectrum monitored at the 572 nm emission that is

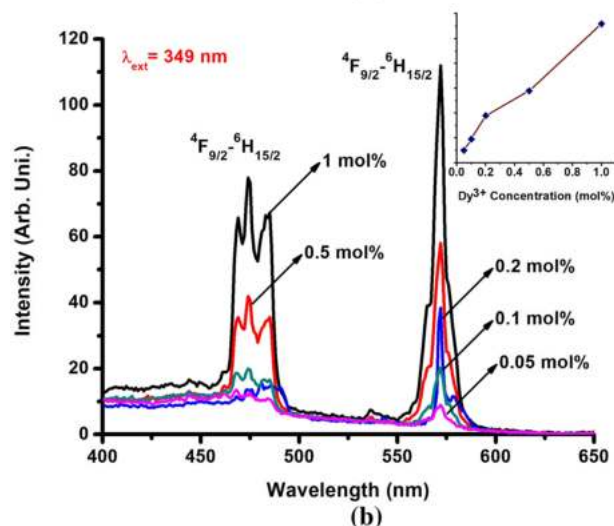
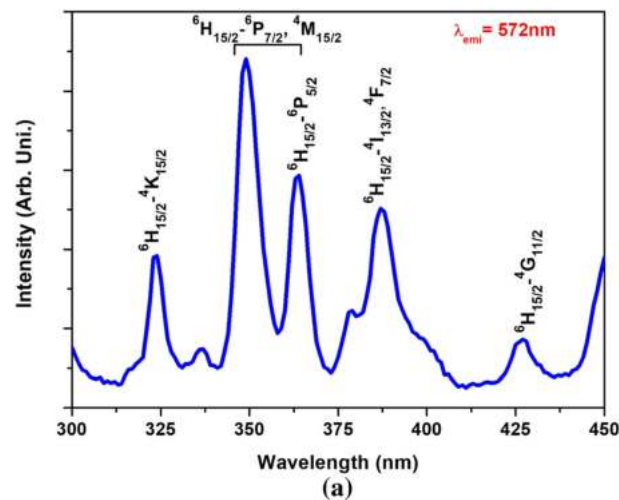


FIGURE 4 Photoluminescence (a) excitation; and (b) emission spectra of the $\text{LiMgBO}_3:\text{Dy}^{3+}$ phosphor

shown in Figure 4(a). Peaks corresponded to ${}^6\text{H}_{15/2} \rightarrow {}^4\text{K}_{15/2}$, [${}^6\text{H}_{15/2} \rightarrow {}^6\text{P}_{7/2}$, ${}^4\text{M}_{15/2}$], ${}^6\text{H}_{15/2} \rightarrow {}^6\text{P}_{5/2}$, [${}^6\text{H}_{15/2} \rightarrow {}^4\text{I}_{13/2}$, ${}^4\text{F}_{7/2}$] and ${}^6\text{H}_{15/2} \rightarrow {}^4\text{G}_{11/2}$ transitions, respectively. The PL emission spectra of Dy^{3+} -doped LiMgBO_3 sample excited at 349 nm wavelength is shown in Figure 4(b). The emission spectra consisted of two peaks centred at 478 nm and 572 nm that were due to the ${}^4\text{F}_{9/2} \rightarrow {}^6\text{H}_{15/2}$ magnetic dipole transition and the hypersensitive ${}^4\text{F}_{9/2} \rightarrow {}^6\text{H}_{13/2}$ electric dipole transitions, respectively of Dy^{3+} [19,20]. Furthermore, the inset in Figure 4(b) shows that emission intensity increased with increase in Dy^{3+} concentration and did not show any concentration quenching until the 1 mol% concentration.

3.4 | Thermoluminescence (TL) studies

TL studies of $\text{LiMgBO}_3:\text{Dy}^{3+}$ were performed after irradiation of the samples with γ -rays and an C^{5+} ion beam. The study included the effect of dopant concentration on the TL glow curves and the effect of dose on TL glow curves, the TL response, the effect of various heating rates and the calculation of trapping parameters.

3.4.1 | TL studies of γ -ray-irradiated $\text{LiMgBO}_3:\text{Dy}$

Effect of concentration on TL glow curves

TL glow curves for $\text{LiMgBO}_3:\text{Dy}^{3+}$ with different Dy^{3+} concentrations, and irradiated with a 200 Gy γ -ray dose are shown in Figure 5. A single glow curve was observed due to one type of defect (luminescent centre) for the prepared phosphor with a glow peak at 160°C. TL glow curves were recorded for 0.05, 0.1, 0.2, 0.5 and 1 mol% concentrations of Dy^{3+} ions in LiMgBO_3 . The concentration profile shown in the inset of Figure 5 shows maximum intensity for 0.1 mol% of Dy^{3+} ions. With further increase in concentration, the intensity decreased, then became constant. The decrease in TL intensity might have arisen due to concentration quenching of Dy^{3+} ions^[21]. With increase in dopant concentration, the distance between the dopant ions decreased, therefore energy levels of dopant ions perturbed each other to quench each other's emission and causing a decrease in the TL intensity^[22]. In the present study, a 0.1 mol% concentration of Dy^{3+} was found to be the best concentration for studying the TL properties, so this was used for further characterization.

Effect of heating rates on TL glow curves

The variation in T_m with various heating rates of $\text{LiMgBO}_3:\text{Dy}^{3+}$ is shown in Figure 6. The glow curve occurred at a lower temperature with a maximum TL intensity for a 2°C/s heating rate. As the heating rate increased from 2°C/s to 12°C/s, the glow curve moved towards the higher temperature side and the intensity continued to decrease. However the shape of the glow curve remained unchanged^[23–25]. The decrease in TL intensity and shift in the peak position towards the higher temperature with increase in heating rate is explained by the theory of thermal quenching^[26,27].

TL response

To study the dose–response of the prepared phosphor, samples were exposed to different doses ranging from 10 Gy to 1.2 kGy γ -rays using

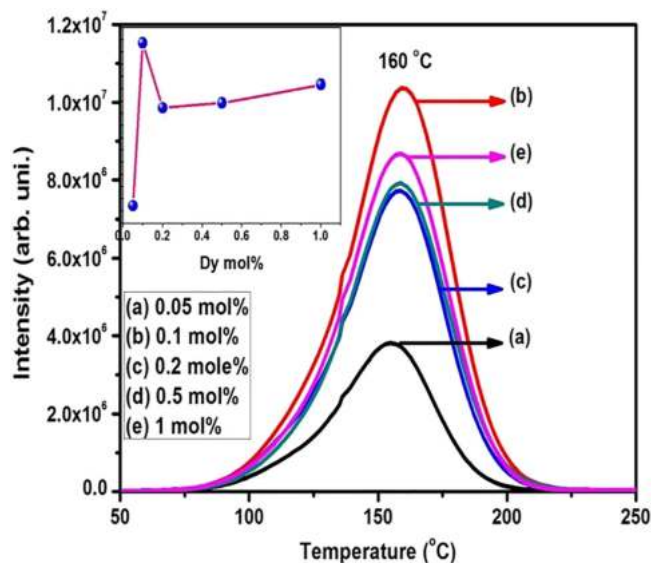


FIGURE 5 Thermoluminescence glow curves for different concentrations of Dy^{3+} in the $\text{LiMgBO}_3:\text{Dy}^{3+}$ phosphor

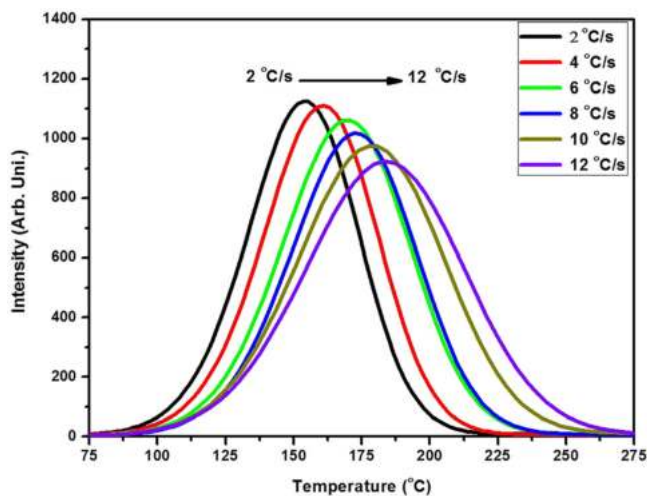


FIGURE 6 Variation of thermoluminescence glow curves of $\text{LiMgBO}_3:\text{Dy}^{3+}$ phosphor with various heating rates

a ^{60}Co source. It was found that the shape and peak temperature of the glow curve remained invariant with varying dose, this is a crucial characteristic for a TLD. Figure 7 shows the TL response of the present phosphor with varying γ -ray doses, the fitted line indicates the linear behaviour of the present phosphor up to a dose of 1 kGy. Further increase in dose resulted in a decrease in intensity and finally saturation at higher doses. This linear TL response can be explained based on the track interaction model^[28,29].

Trapping parameters

In the present study, trapping parameters were calculated to understand the mechanism of TL glow curve in detail. Different methods used were the initial rise method, the whole glow curve method, the various heating rate method, the glow curve convolution deconvolution function and Chen's peak shape method.

(a) Initial rise method Activation energy was estimated using the initial rise method by plotting $\ln(I)$ and $1/kT$, where I is TL intensity, k

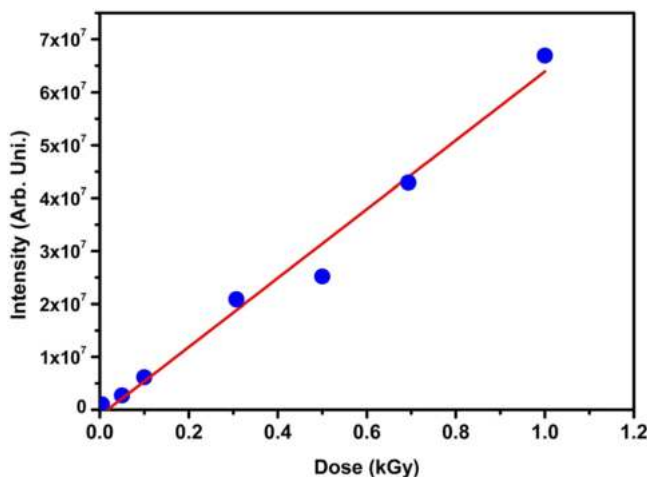


FIGURE 7 Thermoluminescence response of the $\text{LiMgBO}_3:\text{Dy}^{3+}$ phosphor with varying γ -ray doses

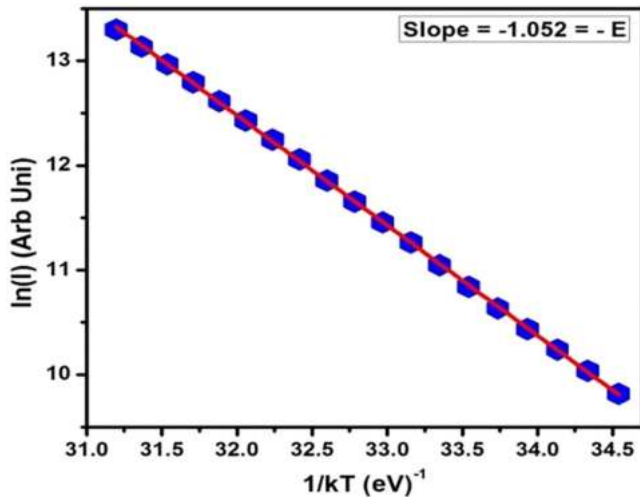


FIGURE 8 Initial rise portion of a single thermoluminescence glow peak for $\text{LiMgBO}_3:\text{Dy}^{3+}$ irradiated with a 10 Gy γ -ray dose

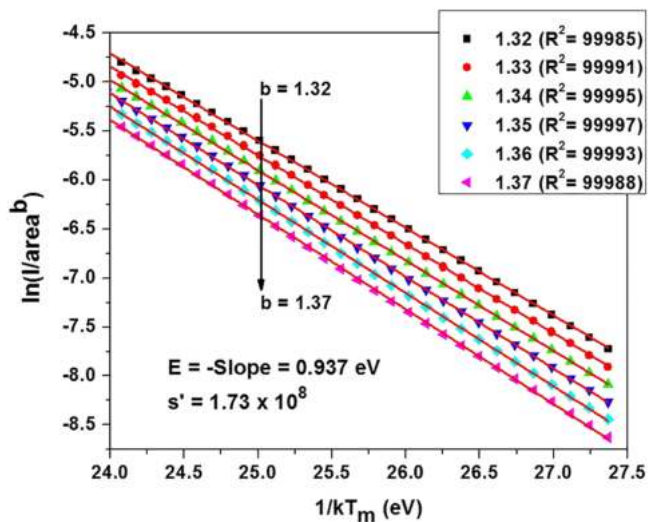


FIGURE 9 Plot of $\ln(I/n^b)$ versus $1/kT$ using the whole glow curve method

is the Boltzmann constant (in eV/K) and T is the temperature in K^[30]. The slope of the curve gives the activation energy E . This method was suggested by Garlic and Gibson^[31]. The rate of retrapping was negligible for the initial rising portion up to a cut-off temperature T_c , for which the TL intensity was 15% less than that of the maximum TL intensity^[32]. Figure 8 shows the initial rise portion of TL glow curve of the sample exposed to a 10 Gy γ -ray dose. The slope of the straight line obtained provided the activation energy E equal to 1.052 eV.

(b) Whole glow curve method The whole glow curve method was used to find the order of kinetics, activation energy and frequency factor^[30]. This method uses an area of peak to find these trapping parameters.

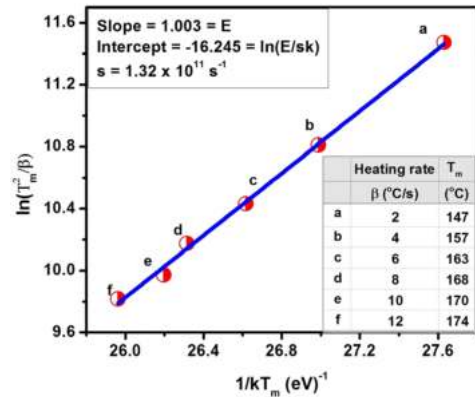


FIGURE 10 Plot of $\ln T_m^2/\beta$ against $1/kT_m$ for the various heating rate method

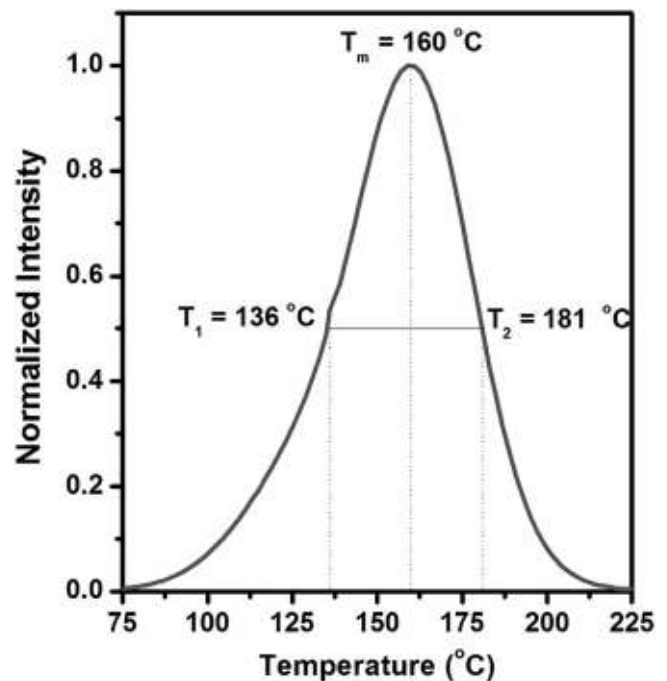


FIGURE 11 Normalized glow curve showing parameters T_1 , T_2 , T_m for Chen's peak shape method

For general order kinetics, the equation is as follows:

$$\ln\left(\frac{I}{n^b}\right) = \ln\left(\frac{s'}{\beta}\right) - \frac{E}{kT} \quad (2)$$

where s' is the effective frequency factor for general order kinetics, β is the heating rate and b is the order of kinetics. For a particular value of b , the plot of $\ln(I/n^b)$ versus $1/kT$ is linear with slope $-E$ and intercept (s'/β) . For the unknown value of ' b ', several lines were drawn to represent different values of b and the best straight line was chosen^[33]. For the present study, Figure 9 shows the plot between $\ln(I/n^b)$ and $1/kT$ for some values of b , out of which

TABLE 2 Trapping parameters for LiMgBO₃:Dy irradiated with γ -rays and using Chen's peak shape method

	α	c_α	b_α	E_α (eV)	s_α (s ⁻¹)
$T_1 = 136^\circ\text{C}$	$\tau = 24$	1.65	1.78	0.978	7.13×10^{10}
$T_2 = 181^\circ\text{C}$	$\delta = 21$	1.32	0	1.013	1.88×10^{11}
$T_m = 160^\circ\text{C}$	$\omega = 45$	3.00	1	1.001	1.35×10^{11}
$\mu_g = 0.47$	$\gamma = 0.88$	Kinetic order $b = 1.42$		Mean $E = 0.997$ eV	Mean $s = 1.31 \times 10^{11}$ s ⁻¹

$b = 1.35$ showed the best linearity. The b value shows that the peaks followed general order kinetics. Activation energy was calculated to be 0.937 eV and the frequency factor was 1.73×10^8 s⁻¹. The results were found to be consistent with the results from the Chen's peak shape method.

(c) Various heating rate method The method of various heating rates was suggested to find the values for the trapping parameters^[24]. The method uses the following relationship:

$$\ln\left(\frac{T_M^2}{\beta}\right) = \frac{E}{kT_M} + \ln\left(\frac{E}{sk}\right) \quad (3)$$

The result suggested that a plot of $\ln T_M^2/\beta$ against $1/kT_M$ with slope E and an intercept of $\ln(E/sk)$ should be linear, from which E and s values can be obtained. Figure 10 shows the plot of $\ln T_M^2/\beta$ against $1/kT_M$. A straight line is obtained and therefore the activation energy was calculated to be 1.003 eV and frequency factor was observed to be 1.32×10^{11} s⁻¹. These results were consistent with those of the Chen's peak shape method.

(d) Chen's peak shape method The activation energy, order of kinetics and frequency factor can also be determined using Chen's general equations^[32,34]. Chen's peak shape method needs three temperature values on the peak: the temperature of the TL maximum, T_m , as well as T_1 and T_2 , which are the temperatures in the ascending and descending parts of the glow curve respectively, for which the TL intensity is a half of the TL at T_m . Figure 11 shows the normalized glow curve with parameters $T_1 = 136^\circ\text{C}$, $T_2 = 181^\circ\text{C}$, and $T_m = 160^\circ\text{C}$ for Chen's peak shape method. Before calculating the kinetic parameters using Chen's equations, some geometrical parameters, τ , δ , ω , were calculated^[17]. The kinetic parameters calculated from this method are given in Table 2. The values of the symmetry factor (μ_g) and the Balarian parameter (γ) were found to be 0.47 and 0.88 respectively

TABLE 3 Comparative study of values of trapping parameters for LiMgBO₃:Dy irradiated with γ -ray using different methods

Method of calculation	E (eV)	s (s ⁻¹)	b
Chen's peak shape	0.997	1.31×10^{11}	1.38
Initial rise	1.052	-	
Various heating rate	1.003	1.32×10^{11}	
Whole glow peak method	0.937	1.73×10^8	1.35
Curve fitting method	P1 0.99 P2 0.98		1.35 1

and indicated the general order characteristic of TL glow curve. From the relationship between kinetic order (b), the geometrical factor (μ) and the Balarian parameter (γ)^[30], the value of kinetic order was found to be 1.42. A comparison of the values for trapping parameters from the Chen's peak shape method and the initial rise method is shown in Table 3. Activation energy value using Chen's peak shape method and the initial rise method are almost the same within experimental errors. The value of activation energy using Chen's peak shape method was somewhat less; this might be due to widening of the glow curve due to the presence of less intense traps and the complex nature of the glow curve^[35], which are sometimes not distinguishable. The frequency factor by both the methods showed good agreement with each other. The order of kinetics found using Chen's peak shape method was found to be 1.42 and suggested that there might be a possibility of retrapping.

(e) Glow curve deconvolution method The trapping parameters of the TL glow curve could be found using the glow curve convolution deconvolution function for first, second, and general order kinetics developed by Kitis *et al.*^[36]. For applying the glow curve convolution deconvolution function to the experimental value, a rough estimation of values of E and b was found using Chen's peak shape method. These values were put in the glow curve convolution deconvolution function and a theoretical curve was generated. The TL glow curve for LiMgBO₃:Dy³⁺ irradiated with a 200 Gy γ -ray dose was deconvoluted to two peaks and is shown in Figure 12. The figure of merit (FOM) value was found to be 1.57 and showed the best fit to the experimental and theoretically generated curve. Activation energy and frequency factor values were found to be consistent with the values obtained from Chen's peak shape method.

Reproducibility

Reproducibility of the synthesized LiMgBO₃:Dy material was studied by carrying out repeated post read-out annealing at 400°C for 10 min, seven times at 50 Gy dose every time. Reproducibility results are shown in Figure 13. It was found that the TL response reduced to less than 10% in first five readouts and then reduced to 23% after seven cycles.

3.4.2 | TL studies of C⁵⁺ ray-irradiated LiMgBO₃

LiMgBO₃:Dy³⁺ samples were irradiated with a 75 MeV C⁵⁺ ion beam and the TL glow curves were studied for different concentrations of Dy and are shown in Figure 14. The glow curve shows two peaks, a prominent peak at 148°C and another at 255°C compared with the TL

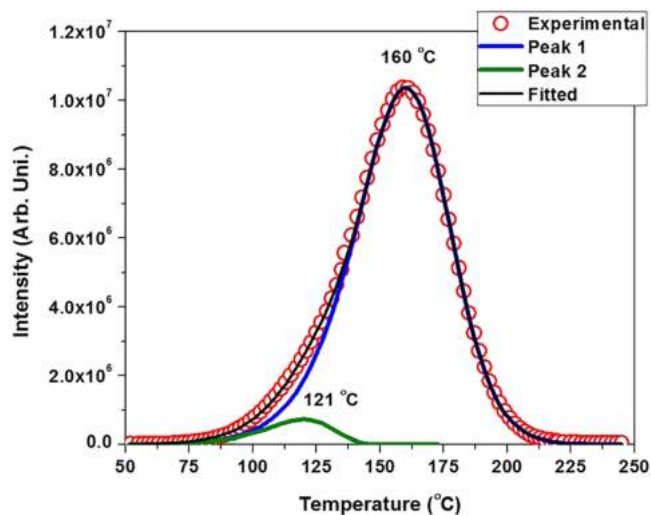


FIGURE 12 Deconvolution of the thermoluminescence glow curve for $\text{LiMgBO}_3:\text{Dy}^{3+}$ irradiated with a 200 Gy γ -ray dose

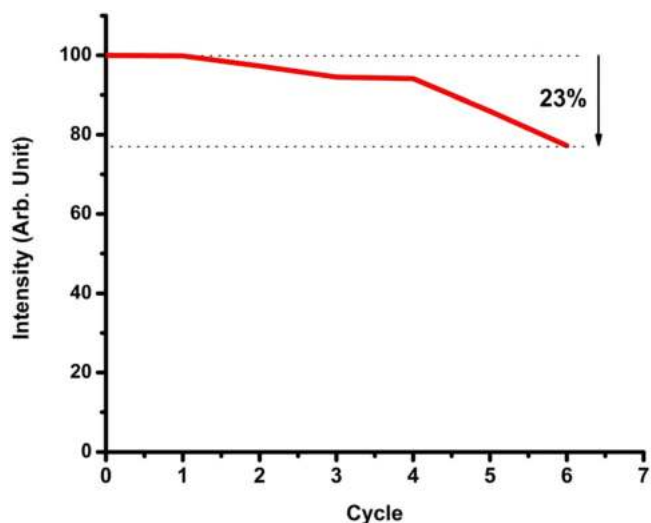


FIGURE 13 Reproducibility of the synthesized $\text{LiMgBO}_3:\text{Dy}$ phosphor

glow curve for γ -ray-exposed samples that showed single peak at 160°C. Heavy carbon ions lost their whole energy after penetrating the phosphor, this action perturbed the normal lattice site and therefore altered the trapping mechanism and resulted in the generation of new trap centres that caused the peak at 255°C^[12,37]. The present phosphor showed a maximum TL intensity at 0.7 mol% of Dy when exposed to the C^{5+} ion beam fluence 1×10^{11} ions/cm². Furthermore, the TL glow curves were observed at different fluence ranges for the C^{5+} ion beam from 2×10^{10} ions/cm² to 1×10^{12} ions/cm², as shown in Figure 15. With increase in fluence up to 1×10^{11} ions/cm², the TL intensity increased and then decreased after further increase. With increase in radiation dose, traps were increasingly filled and then, on thermal stimulation, traps released their charge carriers

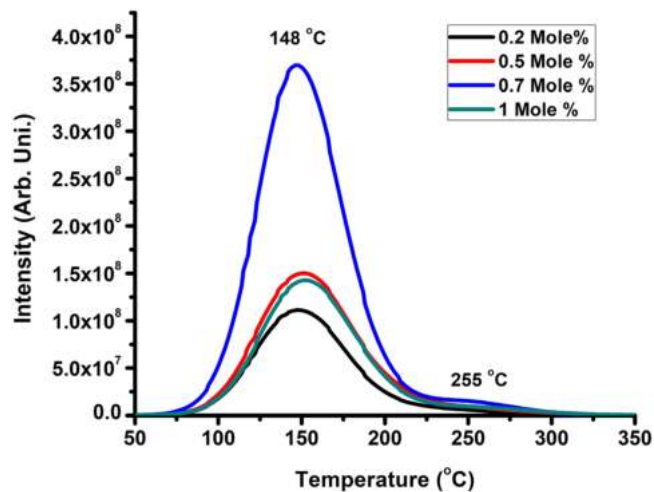


FIGURE 14 Thermoluminescence glow curves recorded for different concentrations of Dy in the $\text{LiMgBO}_3:\text{Dy}^{3+}$ samples exposed to a MeV of C^{5+} ion beam

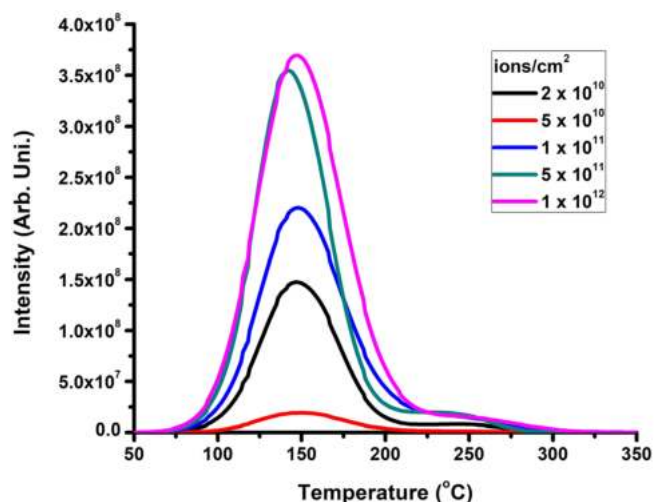


FIGURE 15 Thermoluminescence glow curves of $\text{LiMgBO}_3:\text{Dy}^{3+}$ exposed to different fluence ranges of C^{5+} ion beams

to finally recombine with their counterparts and give rise to an increase in the TL intensity of the glow peak^[38]. The TL response curve for the C^{5+} ion beam-irradiated $\text{LiMgBO}_3:\text{Dy}^{3+}$ samples is shown in Figure 16, which shows that the TL response was linear in the range 2×10^{10} to 1×10^{11} ions/cm² and then decreased. Therefore, the phosphor was useful in the respective range for C^{5+} ion irradiation. Fading of the synthesized material for γ -ray and C^{5+} beam exposure is shown in Figure 17. To study fading, samples were irradiated with 50 Gy for γ -rays and 1×10^{11} ions/cm² for C^{5+} ion beams and then samples were stored for 27 days in the dark. The results in Figure 17 revealed that fading for γ -ray-exposed and carbon beam-exposed sample for first 3 days was approximately 30%, however on fifth day fading remains same for the γ -ray exposed sample but carbon

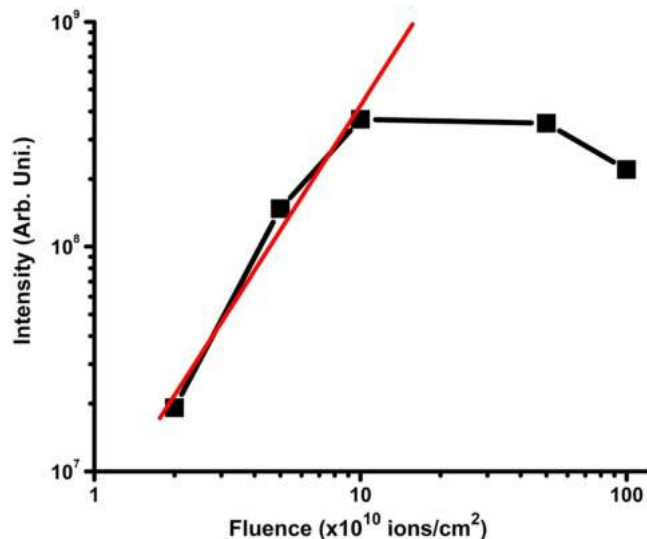


FIGURE 16 Thermoluminescence response curve for C^{5+} ion beam-irradiated $LiMgBO_3:Dy^{3+}$ samples

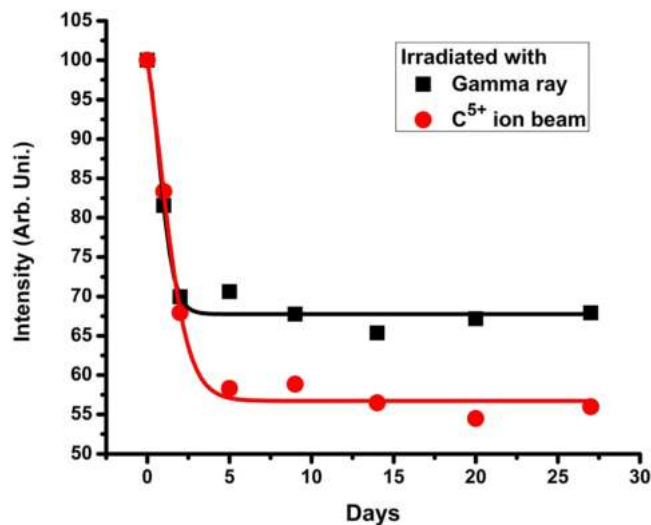


FIGURE 17 Fading of synthesized $LiMgBO_3:Dy^{3+}$ for γ -ray and C^{5+} beam exposure

beam-exposed samples faded to 42%, which was very high for a dosimeter.

The trapping parameters of $LiMgBO_3:Dy$ irradiated with the 75 MeV C^{5+} ion beam were calculated. The TL glow curve for 1×10^{11} ions/cm² fluence of the carbon beam was deconvoluted to three peaks using the glow curve deconvolution method with FOM 1.61% and is shown in Figure 18. The trapping parameters for each peak for all fluencies were calculated and are shown in Table 4.

3.5 | Electron paramagnetic resonance (EPR)

EPR spectra were recorded at room temperature (RT) and liquid nitrogen temperature (LNT). Phosphors were irradiated with a γ -ray dose

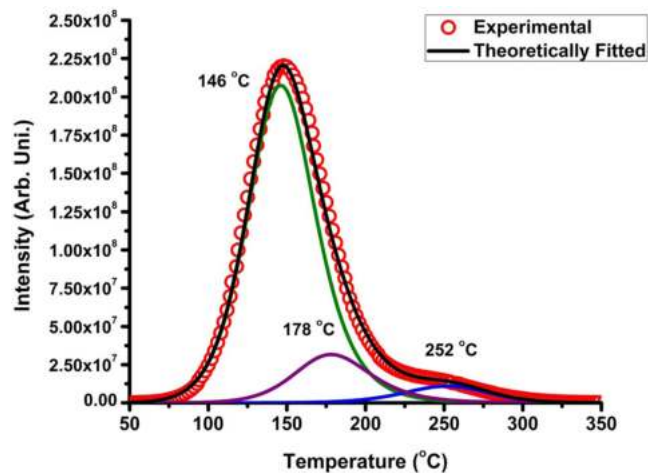


FIGURE 18 Deconvolution of thermoluminescence glow curves for $LiMgBO_3:Dy$ irradiated with a 75 MeV C^{5+} ion beam

TABLE 4 Trapping parameters for $LiMgBO_3:Dy$ irradiated with a 75 MeV C^{5+} ion beam using the glow curve deconvolution method

Fluence (ions/cm ²)	Peak	T _m	E	b
2×10^{10}	P1	146	0.93	2
	P2	170	0.96	2
	P3	249	1.04	1.3
5×10^{10}	P1	146	0.97	1.7
	P2	168	0.98	1.7
	P3	248	1.02	1
1×10^{11}	P1	146	0.92	2
	P2	168	0.99	1.9
	P3	248	1.06	2
5×10^{11}	P1	142	0.95	1.6
	P2	174	0.97	2
	P3	242	1.06	1
1×10^{12}	P1	146	0.95	1.9
	P2	178	1.01	2
	P3	252	1.06	1.5

for EPR studies. EPR studies on Dy^{3+} ions in $YAl_3(BO_3)_4$ and $EuAl_3(BO_3)_4$ aluminoborates, $LiNaSO_4$, $CaMg_2(SO_4)_3:Dy^{3+}$ have been reported recently^[39–41]. It was noted that EPR was observed only at liquid helium temperature, because the electronic configuration of Dy^{3+} ion is $4f^9$ and its ground state, first excited state and second excited states are given by ${}^6H_{15/2}$, ${}^6H_{13/2}$ and ${}^6H_{11/2}$, respectively. Furthermore, ${}^6H_{15/2}$ splits into eight, ${}^6H_{13/2}$ into seven and ${}^6H_{11/2}$ into six Kramer's doublets under very low crystal field symmetry^[41]. The first excited multiplet ${}^6H_{13/2}$ was located $\approx 3.5 \times 10^3$ cm⁻¹ higher in energy. Due to mixing of the higher states and the large orbital angular momentum associated with these states, there was a very short spin lattice relaxation time for the Dy^{3+} ion and therefore EPR was observed^[41].

The non-irradiated $LiMgBO_3:Dy$ sample did not show an EPR signal at RT. The EPR spectrum for γ -ray-irradiated $LiMgBO_3:Dy$ is shown in Figure 19. The RT EPR spectrum consisted of a well resolved

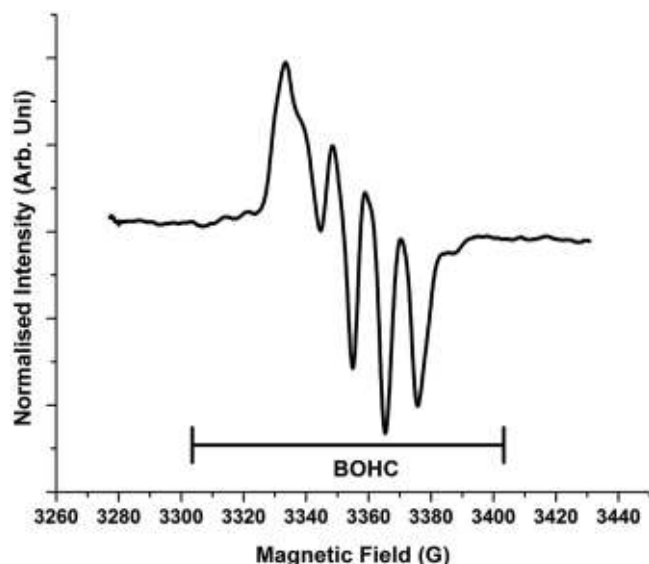


FIGURE 19 Electron paramagnetic resonance spectrum of a polycrystalline sample of γ -ray-irradiated $\text{LiMgBO}_3:\text{Dy}$

quartet structure (perpendicular components) with spacing of 10 G and having nearly equal intensity. Superimposed onto the lowest field component of this quartet structure, a broad parallel-like structure (parallel component) was observed, but without any hyperfine structure. The observed EPR spectrum was assumed to arise from single paramagnetic species having nearly axial symmetry ($g_{\parallel} = 2.020$; $g_{\perp} = 2.0064$, $A_{\parallel} = 0$ G and $A_{\perp} = 10.5$ G). The quartet hyperfine Bohr magnetron structure was due to the interaction of unpaired electrons in the radical with the most abundant isotope of boron, ^{11}B ($I = 3/2$, natural abundance 80.2%). The hyperfine structure due to the ^{10}B nucleus ($I = 3$; isotopic abundance 19.80%) was unresolved due to overlapping of its hyperfine lines^[42] and resulting in significant line-broadening to as much as 5 G. This finding is shown in Figure 19. The experimentally observed $g_{\text{iso}} = 2.0111$ for this radical was close to the g_{iso} value (2.0111) reported in the literature. Based on observed

g values, this signal was attributed to the boron-oxygen hole centre (BOHC) (g for e trapped centres is less than 2.00, whereas for hole-trapped species g is greater than 2.00). The EPR parameters for different types of BOHCs are given in Table 5. EPR parameters for free radicals were precisely determined from the calculated spectra, assuming axial symmetry of g and A tensors, which were obtained using the WIN-EPR BRUKER SIMFONIC program based on perturbation theory^[43]. The theoretical EPR signals were calculated using spin Hamiltonian $H_s = \beta eS \cdot g \cdot B + I \cdot A \cdot S$, where βe is the electron magnetron; S and I are the electron spin and nuclear spin operators, respectively; g is the spectroscopic factor; B is the applied magnetic field; and A is the hyperfine terms for the ^{11}B nucleus^[44]. The possibilities for EPR spectrum generation could be:

(i) The quartet structure arising from the interaction of unpaired electrons with the ^7Li nucleus (^7Li , having a natural abundance of 92.5%) as observed in $[\text{Li}]^0$, but the unpaired spin density resides on the S orbital for this centre, leading to a large hyperfine coupling constant and isotropic $g = 2.0023$.

Howard J. A. and Sutcliffe R. observed three types of $[\text{Li}]^0$ centres with g values close to free electron g value 2.0023 and a large hyperfine coupling constant 135 G in the hydrocarbon matrix. In same system, authors observed evidence for stabilization of the lithium trimer, Li_3 ($A = 33.1$ G and $g = 2.001$)^[45]. However, the small hyperfine coupling constant and g value observed in our case did not support this finding.

(ii) The unpaired spin density on oxygen interacted with ^7Li . Even though there have been many papers on EPR studies on irradiated lithium-based glasses and inorganic matrices, no paramagnetic centre of this type has been reported.

EPR spectra at different temperatures in the range 300–450 K were recorded to identify the role of electron-hole recombination reactions in thermally stimulated luminescence (TSL) processes. Spectra are shown in Figure 20. It was observed that, in the temperature range 400–425 K, there was a drastic reduction in the intensity of the BOHC signal. Furthermore, the BOHC signal became thermally destroyed at 425 K by releasing the trapped hole. The recombination of this hole

TABLE 5 Spin Hamiltonian (g and A) parameters for boron-oxygen hole centres (BOHCs) in different minerals and inorganic matrices (the principal hyperfine coupling constant (a value) for ^{11}B is given in gauss)

Matrix	Radical	g_1	g_2	g_3	g_{ava}	A_1	A_2	A_3	A_{iso}	Temp. (K)	Ref.
CaCO_3	BO_3^{2-}	2.0080	2.0127	2.0127	2.0111	12.6	8.4	8.4	9.8	4.2 K	1
$\text{CaBSiO}_4(\text{OH})$	$[\text{BO}_4]^0$	2.0059	2.0066	2.0512	2.0212	9.2	6.3	4.6	6.7	77 K	2
$\text{CaBSiO}_4(\text{OH})$	$[\text{BO}_4]^0$	2.0031	2.0118	2.0482	2.0210	9.85	9.06	4.01	7.64	10 K	3
$\text{CaB}_2(\text{SiO}_4)_2$	$[\text{BO}_4]^0$	2.0059	2.0066	2.0481	2.0202	9.6	9.4	4.9	7.97	77 K	2
ZrSiO_4	$[\text{BO}_4]^0$	2.0039	2.0013	2.0474	2.0175	4.88	5.19	1.90	3.99	15 K	4
$\text{K}_2\text{B}_2\text{O}_4$	BO_3^{2-}	2.0091	2.0143	2.0128	2.0121	12.37	7.54	7.54	9.15	300 K	5
SrB_4O_7	BO_3^{2-}	1.9950	2.0130	2.0130	2.0070	13.26	9.46	9.46	10.73	300 K	6
BaBPO_5	BOHC	1.9907	2.0133	2.0419	2.0153	8.0	9.0	8.25	8.42	300 K	7
SrBPO_5	BOHC	1.9908	2.0133	2.0416	2.0152	9.0	9.0	8.5	8.83	300 K	8
LiMgBO_3	BOHC	2.0064	2.0064	2.0200	2.0110	–	10.50	10.50	7.0	300 K	Present work ^a

^a CaCO_3 , $\text{CaBSiO}_4(\text{OH})$, $\text{CaB}_2(\text{SiO}_4)_2$ and ZrSiO_4 represents calcite, detolite, danburite and zircon minerals respectively; errors in estimation of g and A values are ± 0.0001 and ± 0.05 Gauss respectively.

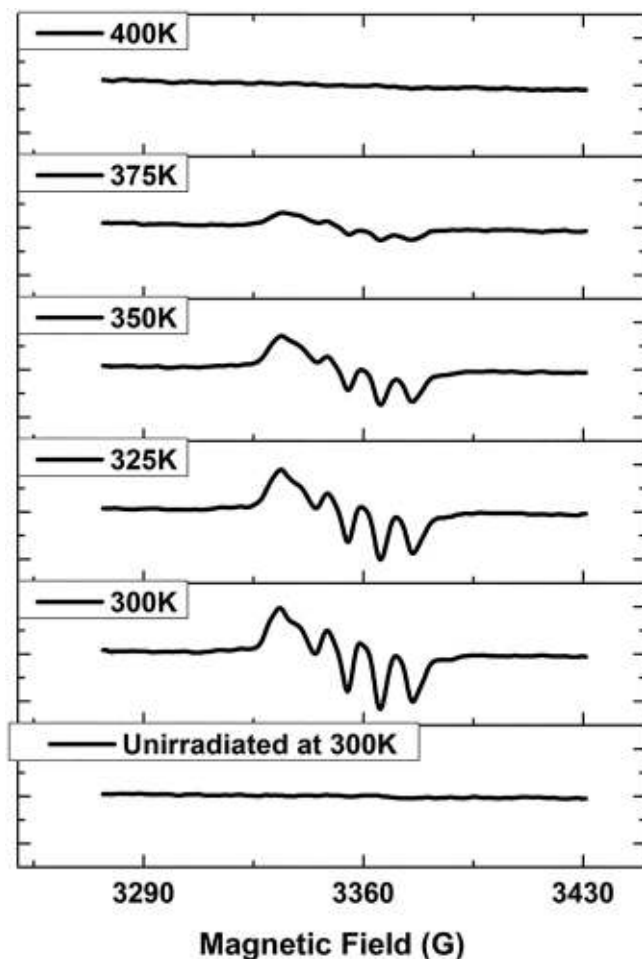


FIGURE 20 Electron paramagnetic resonance spectra of LiMgBO₃:Dy recorded at different temperatures in the range 300–450 K

with electrons resulted in the production of an excited state of Dy³⁺. De-excitation of Dy³⁺ gave its characteristic emission before reaching the ground state, resulting in a glow peak at around 160°C.

4 | CONCLUSIONS

A LiMgBO₃:Dy³⁺ phosphor was prepared using the solution combustion method and different techniques were used to study its luminescence properties. The XRD pattern was found to be consistent with standard patterns and depicted that the pattern belonged to the pure monoclinic phase with space group C2/c. SEM micrographs clearly indicated agglomeration with rod shapes distributed widely. FTIR spectrum showed bands at 1458 cm⁻¹ and 1287 cm⁻¹, corresponding to asymmetrical stretching relaxations of the B–O bond of the trigonal BO₃ unit. PL emission spectra for LiMgBO₃:Dy³⁺ consisted of two peaks centred at 478 and 572 nm due to the ⁴F_{9/2}→⁶H_{15/2} magnetic dipole transition and the hypersensitive ⁴F_{9/2}→⁶H_{13/2} electric dipole transitions of Dy³⁺ respectively. Moreover the γ-irradiated LiMgBO₃:Dy³⁺ sample showed TL linearity in the dose range 10 Gy to 1 kGy and the C⁵⁺-irradiated samples showed TL linearity in the fluence range 2 × 10¹⁰ to 1 × 10¹¹ ions/cm². In the present study, different

methods were used to calculate and compare trapping parameters to understand the mechanism of the TL glow curve in detail. Finally, EPR spectra were recorded at different temperatures to study the role of electron–hole recombinations in the TL process.

ACKNOWLEDGEMENTS

One of the authors, Mangesh M. Yerpude, is thankful to University Grants Commission-India for providing financial assistance to carry out this work under the UGC-NET-JRF scheme (file no. F.17-86/2008 (SA-I)). The authors also would like to thank the Director of the IUAC for providing financial assistance and the ion beam facility for carrying out this work under the IUAC projects. Authors are also thankful to Birendra Singh for support during measurements at IUAC.

ORCID

Vibha Chopra  <https://orcid.org/0000-0003-2849-4332>

S.J. Dhoble  <https://orcid.org/0000-0002-4249-8228>

REFERENCES

- [1] V. Chopra, L. Singh, S. P. Lochab, V. E. Aleynikov, A. S. Oinam, *Radiat. Phys. Chem.* **2014**, *102*, 5.
- [2] V. Chopra, L. Singh, S. P. Lochab, *Nucl. Instrum. Meth. Phys. Res. Section A* **2013**, *717*, 63.
- [3] N. Salah, S. Habib, S. S. Babkair, S. P. Lochab, V. Chopra, *Radiat. Phys. Chem.* **2013**, *86*, 52.
- [4] L. Singh, V. Chopra, S. P. Lochab, *JOL* **2011**, *131*, 1177.
- [5] R. Norrestam, *Zeitschrift für Kristallographie* **1989**, *187*, 103.
- [6] S. R. Anishia, M. T. Jose, O. Annalakshmi, V. Ramasamy, *JOL* **2011**, *131*, 2492.
- [7] Y. Saleh, M. Alajerami, S. Hashim, W. M. Saridan, W. Hassan, A. T. Ramli, A. Kasim, *Phys. B* **2012**, *407*, 2398.
- [8] Z. Liang, F. Mo, X. Zhang, L. Zhou, *JOL* **2014**, *151*, 47.
- [9] N. S. Bajaj, S. K. Omanwar, *Optik-Int. J. Light Elec. Optics* **2014**, *125*, 4077.
- [10] A. K. Bedyal, V. Kumar, R. Prakasha, O. M. Ntwaeaborwab, H. C. Swart, *Appl. Surf. Sci.* **2015**, *329*, 40.
- [11] W. Wesch, A. Kamarou, E. Wendler, *Nucl. Instrum. Methods B.* **2004**, *225*, 111.
- [12] M. M. Yerpude, N. S. Dhoble, S. P. Lochab, S. J. Dhoble, *Luminescence* **2016**, *31*, 1115.
- [13] G. Kraft, *Prog Part Nucl Phys.* **2000**, *45*, S473.
- [14] H. Suit, T. De Laney, S. Goldberg, H. Paganetti, B. Clasio, L. Gerweck, *Radiother. Oncol.* **2010**, *95*, 3.
- [15] M. Scholz, *Nucl Instrum Methods B* **2000**, *161*, 76.
- [16] D. Schulz-Ertner, O. Jäkel, W. Schlegel, *Semin. Radiat. Oncol.* **2006**, *16*, 249.
- [17] D. Kanjilal, S. Chopra, M. M. Narayanan, I. S. Iyer, J. J. R. vandana, S. K. Datta, *Nucl. Instrum. Methods Phys. Res. A* **1993**, *328*, 97.
- [18] N. S. Bajaj, S. K. Omanwar, *Opt. Mater.* **2013**, *35*, 1222.
- [19] A. H. Oza, N. S. Dhoble, S. P. Lochab, S. J. Dhoble, *Luminescence* **2015**, *30*, 967.
- [20] Y. S. Xin, C. Z. Jun, G. L. Xin, W. L. Liang, *Ceram. Int.* **2012**, *38*, 1065.

- [21] A. J. Dekker, *Solid State Physics*, Prentice-Hall Inc., Englewood Cliffs, New Jersey **1957**.
- [22] R. Bharthasaradhi, L. C. Nehru, V. Chopra, S. J. Dhoble, *J. Mater. Sci. Mater. Electron.* **2018**, *29*, 11229. <https://doi.org/10.1007/s10854-018-9209-7>
- [23] A. N. Yazici, *Nucl. Instrum. Methods Phys. Res., Sect. B* **2004**, *215*, 174.
- [24] W. Hoogenstraaten, *Philips Res. Rep.* **1958**, *13*, 515.
- [25] G. Kitis, S. Charalamboust, J. W. N. Tuyn, *J. Phys. D Appl. Phys.* **1993**, *26*, 2036.
- [26] B. P. Kore, N. S. Dhoble, S. J. Dhoble, *Radiat. Meas.* **2014**, *67*, 35.
- [27] S. G. Gorbics, A. E. Nash, F. H. Attix, *Int. J. Appl. Radiat. Isot.* **1969**, *20*, 829.
- [28] S. Mahajna, Y. S. Horowitz, *J. Phys. D Appl. Phys.* **1997**, *30*, 2603.
- [29] Y. S. Horowitz, O. Avila, M. Rodrigues, *Nucl. Instrum. Methods Phys. Res., Sect. B* **2001**, *184*, 85.
- [30] V. Pagonis, G. Kitis, C. Furetta, *Numerical and Practical Exercises in Thermo-luminescence*, Springer, Berlin **2006**.
- [31] G. F. J. Garlick, A. F. Gibson, *Proc. Phys. Soc.* **1948**, *60*, 574.
- [32] R. Chen, *J. Electrochem. Soc.* **1969**, *116*, 1254.
- [33] J. M. Kalita, M. L. Chithambo, *JOL* **2017**, *185*, 72.
- [34] R. Chen, S. A. A. Winer, *J. Appl. Phys.* **1970**, *41*, 5227.
- [35] C. M. Sunta, W. E. Feria Ayta, T. M. Piters, S. Watanabe, *Radiat. Meas.* **1999**, *30*, 197.
- [36] G. Kitis, R. J. M. Gomez, J. W. N. Tuyn, *J. Phys. D Appl. Phys.* **1998**, *31*, 2636.
- [37] M. Bhake, G. B. Nair, G. D. Zade, S. J. Dhoble, *Luminescence* **2016**, *31*, 1468.
- [38] J. A. Wani, N. S. Dhoble, S. P. Lochab, S. J. Dhoble, *Nucl. Instrum. Methods Phys. Res., Sect. B* **2015**, *349*, 56.
- [39] A. A. Prokhorov, E. E. Zubov, L. F. Chernysh, H. Szymczak, A. D. Prokhorov, *Low Temp. Phys.* **2014**, *40*, 939.
- [40] R. T. Weber, *WIN-EPR Simfonia Manual Ver1.2*, Bruker Instruments, Inc., Billerica, MA **1995** and references therein.
- [41] S. Tamboli, R. M. Kadam, B. Rajeswari, B. Singh, S. J. Dhoble, *JOL* **2018**, *203*, 267.
- [42] R. M. Kadam, T. K. Seshagiri, V. Natarajan, S. V. Godbole, *Nucl. Instrum. Methods Phys. Res., Sect. B* **2008**, *266*, 5137.
- [43] K. K. Gupta, R. M. Kadam, N. S. Dhoble, S. P. Lochab, S. J. Dhoble, *Chem. Phys. Lett.* **2018**, *20*, 1540.
- [44] M. Kumar, T. K. Seshagiri, R. M. Kadam, S. V. Godbole, *Mater. Res. Bull.* **2011**, *462*, 1359.
- [45] J. A. Howard, R. Sutcliffe, B. Mile, *Chem. Phys. Lett.* **1984**, *112*, 84.

How to cite this article: Yerpude MM, Chopra V, Dhoble NS, Kadam RM, Krupski AR, Dhoble SJ. Luminescence study of LiMgBO₃:Dy for γ -ray and carbon ion beam exposure. *Luminescence*. 2019;1-12. <https://doi.org/10.1002/bio.3694>